Study of extra wide coherent optical combs generated by a QW-based integrated passively mode-locked ring laser

Optics Letters

Study of extra wide coherent optical combs generated by a QW-based integrated passively mode-locked ring laser

Valentina Moskalenko,[1,*] Jeroen Koelemeij,[2] Kevin Williams,[1] and Erwin Bente[1]

[1]Eindhoven University of Technology, De Zaale, 5612 AJ Eindhoven, The Netherlands
[2]Vrije Universiteit, De Boelelaan 1081, 1081 HV Amsterdam, The Netherlands
*Corresponding author: v.moskalenko@tue.nl

Received 1 February 2017; accepted 20 February 2017; posted 14 March 2017 (Doc. ID 284798); published 31 March 2017

We present an investigation of an InP quantum-well-based integrated extended cavity passively mode-locked laser which shows extra broad frequency comb generation. The ring laser was characterized in frequency and time domains for a range of the current levels injected in the semiconductor optical amplifier. The study showed an increase of the bandwidth to over 40 nm at the −20 dB level. The coherence between the longitudinal modes in the wide comb is demonstrated by the characterization of a spectrally filtered signal in time and RF domains. The relative time delay across the optical comb was measured.

OCIS codes: (140.4050) Mode-locked lasers; (250.4390) Nonlinear optics, integrated optics; (250.5300) Photonic integrated circuits.

https://doi.org/10.1364/OL.42.001428

Optical coherent frequency combs are attractive for many applications in fields of telecommunication [1,2], metrology [3], sensing [4], and microwave generation [5]. To achieve a coherent frequency comb various mode-locking schemes can be used. One of them is passive mode locking. The main advantage of this method is that it does not require an external RF source, and a mode-locking regime can be achieved in relatively simple configuration, which can be realized as a compact photonic integrated circuit (PIC) on a monolithic semiconductor chip. Conventional integrated mode-locked lasers (PMLs) consist of only two sections, namely a semiconductor optical amplifier (SOA) and a saturable absorber (SA). Integrated lasers are very compact. They do not require an optical pump; they can generate pulses with repetition rates of hundreds of gigahertz, and their costs can be reduced when such lasers are fabricated in high volumes. In this Letter, we focus on a study of a passively PML realized in an active-passive InP integration platform. Since both active and passive optical elements can be fabricated on the same chip, this technology allows for more freedom in the design of PMLs, for instance, by including passive waveguides [6], on-chip mirrors [7], phase shifters [8], passive filters [9], and array-waveguide gratings [10] in the laser cavity. Moreover, the capabilities of the active-passive integration platform enable the realization of PICs of higher complexity for particular applications by combining one or more PMLs with other circuitry on the same chip. All the active components in this platform are based on a quantum-well (QW) core. The performance of conventional two-section QW-based PMLs is not as good as that of quantum dash (Q-dash) or quantum-dot (QD)-based lasers. QD and Q-dash lasers show a superior performance in terms of the optical bandwidth, stability, pulse width, and output power [11,12]. A QD-based PML with a 12 nm 3 dB optical bandwidth was presented in [13]. A frequency comb of more than 16 nm was demonstrated from a Q-dash laser in [14]. Previously, we have shown in [15] that by using an extended cavity design for a 20 GHz QW-based PML we can achieve a 3 dB optical bandwidth of 11.5 nm, which was a record value for QW-based PMLs, and it is comparable to the bandwidth of QD-based PMLs. In this Letter, we present an extended cavity ring PML which was fabricated using the same integration platform, as presented in [15]. We present a 12 GHz QW-based PML that generates an extra-wide coherent optical comb, which is wider in width to those from Q-dash lasers. The reasons for such a difference in performance between the PML presented here and the PML presented in [15] will be discussed.

As it will be shown later, the optical comb produced is not flat, however it could still allow for using the PML in various applications, for example, for terahertz generation. The optical comb of more than 40 nm at the −20 dB level was observed. For reference, 20 dB linewidth of the comb demonstrated in [14] was in the order of 25 nm.

In order to prove coherence between all modes of the comb shown in this Letter, we present a series of measurements in time and frequency domains. Moreover, we examine the chirp of the output pulses by measurements of relative time delay between the spectral components of the comb [16].

The passively mode-locked ring laser was designed as an InP PIC using a library of standardized building blocks and was fabricated within a multiproject wafer run in the COBRA active-passive integration platform. The platform uses shallowly and deeply etched ridge waveguides that are 2.0 and 1.5 μm

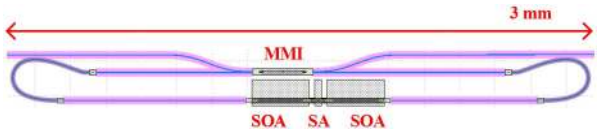

Fig. 1. Mask layout of 12 GHz ring PML.

wide, respectively, and butt-joint technology with one regrowth step and one overgrowth step to achieve the active-passive integration. The layer stack has a 500 nm thick InGaAsP $Q = 1.25$ waveguiding layer. The mask layout of the PML is shown in Fig. 1.

The laser cavity is formed by two SOA sections of 325 μm, a 40 μm long SA section and deeply (curved) and shallowly (straight) etched passive waveguides. The SA was 30 long. The light is coupled out using a 2 × 2 multimode interference coupler (MMI). In order to avoid back reflections coming from the edge of the chip, the output waveguides were 7° tilted in respect to the facet. The intracavity reflections were reduced by using angled active-passive interfaces, adiabatic bends, an optimized MMI structure, and optimized deep to shallow waveguide transitions.

The laser geometry supports two counter-propagating pulses that interact within the SA, simultaneously saturating it. This so-called symmetrical ring colliding pulse geometry allows us to reduce the signal intensity inside the SOA but, at the same time, provide full optical power to the SA. This is particularly beneficial in comparison with the linear configuration of PMLs due to the less saturated gain which is in favor of stable mode-locking operation [17].

The chip with the laser was placed on an aluminum sub-carrier, and electrical contacts were wire-bonded to a printed circuit board. The results presented here were obtained when the sub-carrier was water cooled to 18°C. The PML was operated by the current injected in the SOAs, and reverse bias was applied on the SA. The light out of the chip was coupled using an AR coated lensed fiber which was connected to the instruments through the optical isolator to avoid back reflections. The experimental setup is shown in Fig. 2.

The device was characterized in four ways: by measuring the optical spectrum, the RF spectrum of the signal from a photodiode, a time trace produced in a sampling oscilloscope (SO), and autocorrelation. The optical spectrum was measured using a 20 MHz resolution optical spectrum analyzer (OSA). RF beat tones were produced in a 50 GHz photodetector (PD) and recorded using an electrical spectrum analyzer (ESA). The amplified electrical signal from the PD divided by a 1/10 frequency

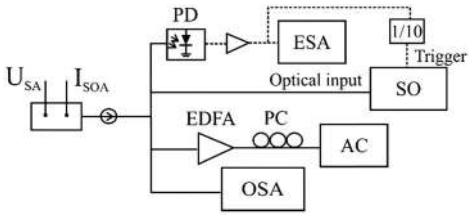

Fig. 2. Experimental setup used for the PML characterization. PD, photodetector; ESA, electrical spectrum analyzer; SO, sampling oscilloscope; EDFA, erbium-doped fiber amplifier; PC, polarization controller; AC, autocorrelator; OSA, optical spectrum analyzer.

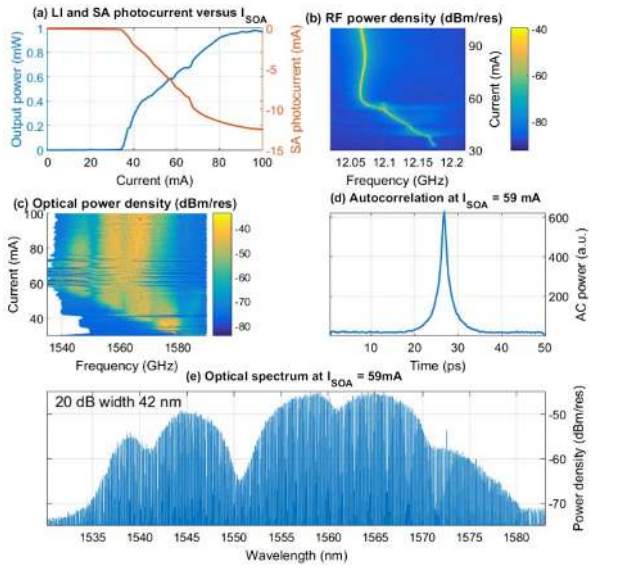

Fig. 3. (a) Fiber-coupled optical power and photocurrent generated in the SA as a function of the SOA current $U_{SA} = -3.4$ V. (b) RF spectra for the range of $I_{SOA} = 35:100$ at $U_{SA} = -3.4$ V. (c) Optical spectra for the same operating conditions as in (b) and (a). (d) Example of autocorrelation for $I_{SOA} = 59$ mA. The autocorrelation full width at half-maximum is 2.0 ps.

divider was used as a triggering signal for the SO with a 30 GHz bandwidth photo receiver. In order to record autocorrelation traces, the signal was first passed through the erbium-doped fiber amplifier (EDFA) and the polarization controller. The configuration of the output waveguides allowed for the signal to be collected from both facets. The signals coupled from both directions show similar performance in terms of coupled optical power, distribution of optical modes, and RF spectrum. All results presented below were obtained for the signal collected from the same facet.

In addition, the optical power and photocurrent generated in the SA were measured as a function of the current injected into the SOA. The dependencies measured at $U_{SA} = -3.4$ V are shown in Fig. 3(a). The lasing threshold for this voltage was observed at $I_{SOA} = 36$ mA. At the injected currents above 80 mA, the curves indicate thermal rollover.

Figures 3(b) and 3(c) show the evolution of the RF spectrum around the fundamental frequency and the optical spectrum with the SOA current. An increase of the SOA current up to around 66 mA results in a decrease of the fundamental frequency and dramatic reshaping of the optical spectrum. Above 65 mA, the behavior stabilizes, and no significant changes are observed. As discussed in [18], repetition frequency tuning occurs due to variation in the saturation processes inside the SA and SOA when the pulse intensity is changing. The time variation of the gain and absorption also can result in a distortion of the optical spectrum [19] due to the self-phase effect in both the SA and SOA. For instance, in [20], it was shown that self-phase modulation effects in an SOA result in an oscillatory shape of the optically amplified pulse spectrum. The effect increases with an increase of the pulse intensity. Similar observations have been made in our case. An increase of the optical power leads to the appearance of spectral wings on the high

energy side from the spectral peak. Above 66 mA, the spectral shape remains relatively stable, which we attribute to a stabilization of the peak intensity of the pulse. For the same reason, above 66 mA, significant variation of the repetition frequency was not observed.

We expect that the reason for such a broad optical comb can be the high intracavity peak power of the pulse. In [15], we presented a 20 GHz PML which was realized in the colliding-pulse ring geometry. This laser had a shorter cavity length, the same length of the SOAs and a 30 μm long SA. Even though a similar geometry was used, the PML presented in [15] showed a more than twice narrower bandwidth (below 20 nm at 20 dB level); the threshold current was more than 70 mA which is two times higher, and the optical power was almost 3 dB lower than the one presented here at the same current levels. Notice that the laser presented in [15] was operating at higher repetition rates. This means that the peak intensity of the pulse in the case of PML in this Letter is more than three times higher.

One of the reasons for such an increased peak power can be an improved quality of the integration technology used. The electrical contacts were showing a decreased series resistance from $3.8 \cdot 10^{-3}$ to $2.9 \cdot 10^{-3}\ \Omega \cdot \mathrm{m}$, which results in a reduction in heat dissipation and a higher net gain.

Operation at a different temperature can lead to a significant difference in performance such us different central wavelength [21]. The PML described here operates around 1565 nm which is a 20 nm longer wavelength than the operating wavelength of the previous PML. The small signal absorption of the SA is strongly wavelength dependent and, as was shown in [22], can increase by more than two times within this spectral range. Thus, the reduced absorption of the SA leads to the increased peak power which, consequently, leads to the stronger self-phase modulation and the appearance of additional spectral components in the optical spectrum.

The pulse formation was confirmed by the measurements of the AC trace and time trace in the SO. An example of the AC trace is shown in Fig. 3(d). The AC trace width at half-maximum is 2 ps. However, the signal was sent through the EDFA first. The EDFA covers the C and L bands but, at 1565 nm, it has a dip in its amplification spectrum. The signal produced by the PML covers a spectral range from 1530 to 1580 nm. Thus, the EDFA can significantly distort the pulse due to the inhomogeneous gain and, in addition, a dispersion caused by the pulse propagation through 42 m of low-noise C + L band erbium-doped fiber. Therefore, AC measurements can be used only for a confirmation of pulse formation.

Since the observed optical comb has an oscillatory shape, the width measured at 3 dB level is below or comparable to state-of-the-art values reported in [15,23]. However, at −20 dB level the width reaches more than 40 nm which exceeds the measurements made with Q-dash lasers [14]. Figure 3(e) shows an example of the optical comb with the width of 42 nm measured at 20 dB below the top, measured at the same conditions as Fig. 3(d).

In order to examine the coherence across the optical comb, the following measurements were performed. First, we characterized the RF spectrum of the signal which was sent through the tunable bandpass filter (BPF) of 1.5 nm bandwidth. The BPF is able to filter out around 10 longitudinal modes. The results of these measurements are presented in Fig. 4.

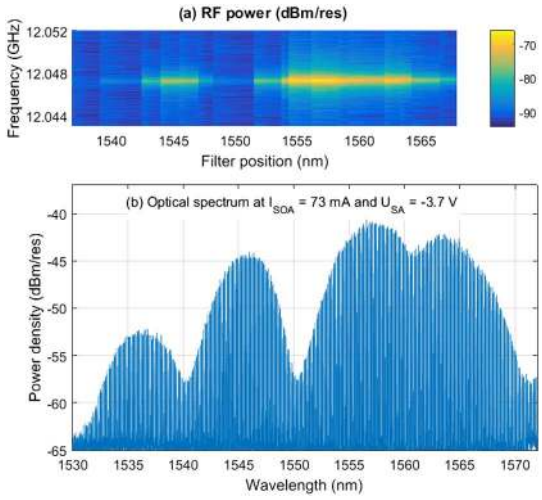

Fig. 4. (a) RF spectrum as a function of the BPF position measured at $I_{SOA} = 73$ mA and $U_{SA} = -3.7$ V. (b) Optical spectrum measured for the same operating conditions as (a).

Figure 4(a) shows RF spectra depending on the spectral position of the tunable filter. Figure 4(b) shows the optical comb which was investigated. The RF peak position showed an increase of 200 kHz across the comb, which might be attributed to a temperature drift, since the measurements took around 1 h. As can be seen from Fig. 4(a), the position of the fundamental RF peak does not show significant variation. This stability indicates that all the spectral components are locked at the same frequency. Moreover, the height of the RF peak as a function of the filter wavelength is very similar to the variation of the optical power across the comb. From this, one can conclude that there is no significant loss of coherence at the edges of the comb, and the comb is not formed by several mutually incoherent combs, as was observed in [24].

In order to investigate the chirp of the optical comb, the measurements of the relative time delay between the spectral components were studied.

The principle of these measurements is similar to the one presented in [16]. In this method, the output signal from the PML was divided into two parts. The first part is used as a trigger signal for the SO, as is shown in Fig. 2 (upper branch). The signal from the second path passes through the BPF of 1.5 nm bandwidth to the SO and other instruments (OSA and AC). By tuning the BPF across the comb, a relative time delay between spectral components can be measured. Moreover, in the same time, the AC traces of the filtered signal were measured.

Figure 5(a) shows a time trace using the full spectral bandwidth measured at $I_{SOA} = 90$ mA and $U_{SA} = -3.5$ V using the 30 GHz SO. The period of the time signal produced is around 80 ps which corresponds to the round-trip time of the cavity. The RF spectrum of the same operating point is depicted in Fig. 5(b) and, in detail, in Fig. 5(c). The power ratio between the peak at the fundamental frequency and noise of the low frequency components is more than 40 dB. The linewidth of the fundamental peak measured at the 10 dB level is 390 kHz. The width of the autocorrelation trace of the non-filtered signal was 1.9 ps. Measured AC traces of the filtered

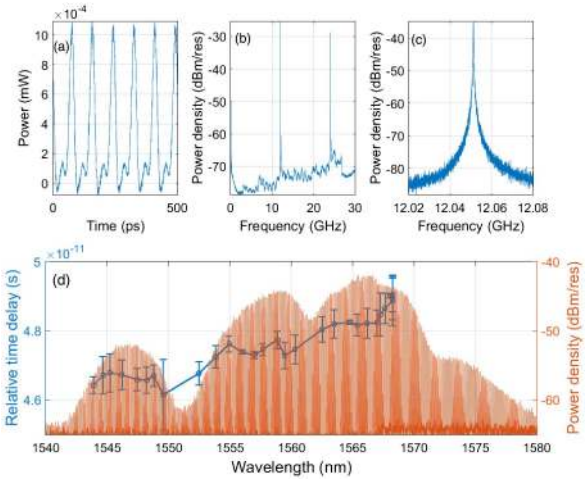

Fig. 5. (a) Time trace recorded in the 30 GHz SO. (b) and (c) RF spectra in a wide and narrow scale. (d) Optical comb (right scale) and the relative time delay (left scale). All data were obtained under $I_{SOA} = 90$ mA and $U_{SA} = -3.5$ V.

tuned signal demonstrated pulse formation across the comb and therefore also confirmed the spectral coherence of the comb. The coherence was confirmed further by the measurements of the time trace of the filtered signal using the SO. The pulses were observed across the whole spectral range.

Figure 5(d) shows the optical spectrum (orange) and relative phase delay (blue) measured at the same operating conditions as Figs. 5(a)–5(c). The total time delay over 25 nm is 2.3 ps, which corresponds to a chirp of 0.09 ps/nm. The optical path from the laser to the SO included a total length of 4 m of single mode fiber. The dispersion of such a fiber is 17 ps/nm/km. The dispersion of the InP/InGaAsp output waveguide can be neglected. Therefore, the contribution to the time delay from the optical components outside the laser cavity is 1.7 ps.

A study of the coherent optical comb generated by a 12 GHz passively mode-locked ring laser is presented. We demonstrate that QW-based passively PMLs can generate coherent optical combs wider than those demonstrated by QD and Q-dash PMLs.

First, the laser was characterized under a range of injected currents. It was shown that an increase of the injected current leads to the broadening of the optical combs. An optical comb of 42 nm width measured at −20 dB level from the top was achieved.

Previously, in [15], we presented a ring 20 GHz PML fabricated within the same integration platform. This laser showed a flat frequency comb with a less than half the width of the laser presented here. Moreover, the PML presented in this Letter showed reduced threshold currents and an almost twice higher output power at the same injected current levels. We explain this increased performance by a decrease in resistance of the electrical contacts and a decrease in SA absorption of the SA due to the fact that the PML is operating at a longer wavelength than the one in [15].

In this Letter, by measuring the RF signal, autocorrelation, and time traces using a SO, we confirm the coherence across the whole width of the optical comb. A time delay of 2.3 ps was measured across optical comb.

Funding. Stichting voor de Technische Wetenschappen (STW) (Memphis II project 13533) "Chipbased optical frequency combs."

Acknowledgment. The authors would like to acknowledge support by the Stichting voor de Technische Wetenschappen (STW) (Memphis II project 13533) "Chipbased optical frequency combs."

REFERENCES

1. M. Mielke and P. J. Delfyett, in *The 14th Annual Meeting of the IEEE Lasers and Electro-optics Society (LEOS)* (2001), Vol. **2**, pp. 713–714.
2. E. A. De Souza, M. C. Nuss, W. H. Knox, and D. A. B. Miller, Opt. Lett. **20**, 1166 (1995).
3. R. Holzwarth, M. Zimmermann, T. Udem, and T. W. Hansch, IEEE J. Quantum Electron. **37**, 1493 (2001).
4. J. Mandon, G. Guelachvili, and N. Picqué, Nat. Photonics **3**, 99 (2009).
5. P. Acedo, G. Carpintero, A. R. Criado, C. de Dios, and K. Yvind, Microw. Opt. Technol. Lett. **54**, 1416 (2012).
6. Y. Barbarin, E. Bente, M. J. R. Heck, J. P. J. M. Rorison, Y. S. Oei, R. Notzel, and M. K. Smit, in *Proceedings of the 13th European Conference on Integrated Optics (ECIO)* (2007).
7. C. Gordón, R. Guzmán, V. Corral, X. Leijtens, and G. Carpintero, Opt. Express **23**, 14666 (2015).
8. S. Latkowski, V. Moskalenko, S. Tahvili, L. Augustin, M. Smit, K. Williams, and E. Bente, Opt. Lett. **40**, 77 (2015).
9. V. Moskalenko, J. Javaloyes, S. Balle, M. K. Smit, and E. A. J. M. Bente, IEEE J. Quantum Electron. **50**, 415 (2014).
10. G. Carpintero, C. Gordon, R. Guzman, X. Leijtens, F. Van Dijk, G. Kervella, M. J. Fice, K. Balakier, and C. C. Renaud, Proc. SPIE **9357**, 935719 (2015).
11. M. G. Thompson, A. R. Rae, M. Xia, R. V. Penty, and I. H. White, IEEE J. Sel. Top. Quantum Electron. **15**, 661 (2009).
12. K. Merghem, C. Calò, R. Rosales, X. Lafosse, G. Aubin, A. Martinez, F. Lelarge, and A. Ramdane, IEEE J. Quantum Electron. **50**, 275 (2014).
13. R. Rosales, K. Merghem, A. Martinez, A. Akrout, J. P. Tourrenc, A. Accard, F. Lelarge, and A. Ramdane, IEEE J. Sel. Top. Quantum Electron. **17**, 1292 (2011).
14. R. Rosales, S. G. Murdoch, R. T. Watts, K. Merghem, A. Martinez, F. Lelarge, A. Accard, L. P. Barry, and A. Ramdane, Opt. Express **20**, 8649 (2012).
15. V. Moskalenko, S. Latkowski, S. Tahvili, T. de Vries, M. Smit, and E. Bente, Opt. Express **22**, 28865 (2014).
16. M. S. Tahvili, L. Du, M. J. R. Heck, R. Nötzel, M. K. Smit, and E. A. J. M. Bente, Opt. Express **20**, 8117 (2012).
17. E. A. Avrutin, J. H. Marsh, and E. L. Portnoi, IEE Proc. **147**, 251 (2000).
18. S. Arahira and Y. Ogawa, IEEE J. Quantum Electron. **33**, 255 (1997).
19. H. A. Haus, IEEE J. Quantum Electron. **11**, 736 (1975).
20. N. A. Olsson and G. P. Agrawal, Appl. Phys. Lett. **55**, 13 (1989).
21. P. M. Stolarz, J. Javaloyes, G. Mezosi, L. Hou, C. N. Ironside, M. Sorel, A. C. Bryce, and S. Balle, IEEE Photon. J. **3**, 1067 (2011).
22. V. Moskalenko, K. A. Williams, and E. A. J. M. Bente, IEEE Photon. J. **8**, 1 (2016).
23. J. S. Parker, R. S. Guzzon, E. J. Norberg, A. Bhardwaj, P. R. A. Binetti, and L. A. Coldren, IEEE J. Quantum Electron. **48**, 114 (2012).
24. E. A. Viktorov, T. Habruseva, S. P. Hegarty, G. Huyet, and B. Kelleher, Phys. Rev. Lett. **112**, 224101 (2014).